Modeling of Heat and Mass Transport in Wall-Cooled Tubular Reactors

G. W. KONING, A. E. KRONBERG and W. P. M. van SWAAIJ

University of Twente, Faculty of Chemical Technology, P.O. Box 217, 7500 AE Enschede (The Netherlands)

E-mail: gwkoning@hetnet.nl

Abstract

Heat transfer experiments with and without chemical reaction were performed in a wall-cooled tubular reactor. The oxidation of carbon monoxide over a CuO/γ-alumina catalyst was used as a model reaction. A two-dimensional heterogeneous reactor model was used for calculation of the temperature and concentration profiles inside the packing. The experiments were performed at Re between 200 and 1400, reactor pressures of 3, 5.9 and 8 bar, wall temperatures of 156, 180 and 200 °C and CO inlet concentrations ranging from 0.1 to 1.5 % vol. The obtained data show that a radial distribution of the axial fluid velocity should be taken into account to reconcile the effective heat transport parameters obtained from experiments with and without reaction.

INTRODUCTION

For a proper design of a wall-cooled tubular reactor an accurate knowledge of the heat transfer properties of the catalyst bed is required because of the high parametric sensitivity of the reactor behavior towards these parameter, especially at conditions near runaway. Nowadays most cooled tubular reactors are not designed on the basis of kinetic data and model calculations, but experiments are carried out using single tubes in pilot scale reactors at conditions similar to those if the industrial process. Previous studies of heat transport phenomena in wall-cooled tubular reactors have shown a discrepancy between the effective radial conductivities of the catalyst bed measured with and without reaction [1–4].

Schwedock [3] found that the effective radial thermal conductivity was about 50 % higher in the presence of reaction than when no reaction occurs. Borman *et al.* [4] used partial oxidation of ethylene to ethylene oxide over a silver/γ-alumina catalyst in their work. The main disadvantages of this reaction system is its complicated kinetics, caused by the occurrence of complete combustion of ethylene as a parallel reaction, the large number of reactants that influence the reaction rate and a slow deactivation of the catalyst. This investigation is a continuation of their work using a more simple reaction system. The oxidation of carbon monoxide to carbon dioxide over a copper oxide catalyst supported on γ-alumina has been chosen as model reaction. An advantage of this reaction is its large enthalpy of reaction of 283 kJ mol^{-1}, which causes a large temperature increase at a small change in the composition of the gas mixture. The kinetics of this reaction was studied separately using an integral and an internal-recycle reactor.

REACTOR MODEL

The reactor model used is commonly referred to in literature as a 'two-dimensional heterogeneous model without axial dispersion', in which the heat and mass balance equations

and their boundary conditions are the following:

Heat balance

$$\varepsilon\rho_f c_{p,f}\frac{\partial T_f}{\partial t} = \frac{1}{r}\frac{\partial}{\partial r}\left(\lambda_{e,r} r \frac{\partial T_f}{\partial r}\right) - u\rho_f c_{p,f}\frac{\partial T_f}{\partial z} + \alpha_p a(T_s - T_f) \quad (1)$$

$$(1-\varepsilon)\rho_s c_{p,s}\frac{\partial T_s}{\partial t} = -\alpha_p a(T_s - T_f) + \sum_{i=1}^{n} -\Delta H_i R_i(c_s, T_s) \quad (2)$$

Mass balance component j

$$\varepsilon\frac{\partial c_f^j}{\partial t} = \frac{1}{r}\frac{\partial}{\partial r}\left(D_{e,r}^j r \frac{\partial c_f^j}{\partial r}\right) - u\frac{\partial c_f^j}{\partial z} + k_g^j a\left(c_s^j - c_f^j\right) \quad (3)$$

$$(1-\varepsilon)\frac{\partial c_s^j}{\partial t} = \sum_{i=1}^{n} -\nu^j R_i\left(c_s^j, T_s\right) - k_g^j a\left(c_s^j - c_f^j\right) \quad (4)$$

$$z = 0,\quad T = T_0,\quad c = c_0 \quad (5)$$

$$r = 0,\quad \frac{\partial T}{\partial r} = 0,\quad \frac{\partial c}{\partial r} = 0 \quad (6)$$

$$r = R_t,\quad -\lambda_{e,r}\frac{\partial T}{\partial r} = \alpha_w(T - T_w),\quad \frac{\partial c}{\partial r} = 0 \quad (7)$$

$\lambda_{e,r}$ and α_w are the effective radial thermal conductivity and wall heat transfer coefficient. All the transport parameters in the model depend on the physical properties of the fluid and the solid and of the flow conditions inside the reactor. $D_{e,r}^j$ is the effective radial dispersion coefficient of component j. The general form of correlations for the dependence of $\lambda_{e,r}$ on the system parameters is:

$$\lambda_{e,r} = \lambda_r^0 + \lambda_r^f \quad (8)$$

The static contribution λ_r^0 depends on bed properties as particle shape and porosity, and on the thermal conductivity of the solid and the fluid. Well-known are the predictive correlations of Yagi and Kunii [5] and Bauer and Schlünder [6]. The contribution of fluid flow, which is the result of mixing of fluid elements moving with different velocities, is usually expressed as function of the fluid Peclet number:

$$\frac{\lambda_r^f}{\lambda_f} = \frac{Pe_h^0}{Pe_{h,r}^\infty};\quad Pe_h^0 = \frac{u_0(\rho c_p)_f d_p^e}{\lambda_f} = RePr \quad (9)$$

$Pe_{h,r}^\infty$ is the Peclet number at fully developed turbulent flow and is a function of the tube-to-particle diameter ratio [7–9]. Distinguishing of heat conduction through the solid and the fluid phase, as is often made in literature, is not applied here. Direct heat transfer through the solid-solid contacts is usually of little importance and cannot be estimated accurately except for beds of particles of simple shape, consisting of certain materials, for which the contact area can be calculated [6]. Particle-to-particle heat transfer occurs mainly through the fluid phase in the interstices between the particles [10] and can therefore not be separated from the fluid-phase contribution.

The wall heat transfer coefficient is usually expressed in the form of a wall Nusselt number as:

$$Nu_w = C_1 + C_2\,Re^{n_1}Pr^{n_2} \quad (10)$$

with n_2 close to 1/3 and n_1 between 0.5 and 1. The flow-independent contribution C_1 is often omitted. The wall heat transfer coefficient is also expressed as in the form of a Biot number, for which Dixon and Creswell [11] propose the following correlation:

$$Bi = \frac{\alpha_w R_t}{\lambda_{e,r}} = 1.5N Re^{-0.25} \quad (11)$$

Literature agrees on the fact that correlations for Nu_w obtained by simultaneous optimization of $\lambda_{e,r}$ and α_w to fit the model prediction to the experimental data differ greatly. One possible explanation, based on heat transfer investigations not discussed in this paper, is the neglecting of the influence of the wall roughness, which is recognized as an important parameter in heat exchanger design. It was found that the resistance of a quasi-stagnant fluid film at the reactor wall accounts for 70 % for the total resistance to heat transfer for $Re > 500$. In case the distribution of the axial fluid velocity over the radius is non-uniform due to variation of the local porosity over the radius, $\lambda_{e,r}$ and $D_{e,r}$, as well as the fluid-to particle heat and mass transfer coefficient α_p and k_g^j will be a function of the radial position.

EXPERIMENTAL

Fluid and catalyst temperatures were measured by 32 thermocouples inside a 1 m reactor with an internal diameter of 53 mm. A scheme of the reactor is shown in Fig. 1. The 0.5 mm type K thermocouples were fixed to a 'thermocouple ladder' placed inside the reactor tube prior to filling it with catalyst. The ladder consists of two 1 mm metal wires resting on the trough-shaped feed distributor, in between which crosses of glass-fiber reinforced polyether-ether-keton crosses are clamped. The thermocouples protrude 5 mm from the holes that are drilled in these crosses. Fluid temperatures were measured at 0, 8, 15, 21 and 25 mm from the centerline of the reactor at 6 axial positions. Close to the centerline, the temperature of a catalyst particle was measured by a thermocouple inserted into a 0.5 mm hole drilled in it. At 8 axial positions, a sample was withdrawn (100 ml min^{-1}) for analysis of the fluid composition. The concentrations of CO and CO_2 in the samples was measured by two infrared analyzers (Mayhak) put in series.

The reactor feed consists mainly of air, which was supplied by a centrifugal compressor at a maximum flow rate of 600 Nl min^{-1} at a pressure of 10 bar. The water content of the air was fixed at a concentration of 1400 ppm by passing it through a heat exchanger. After cooling, excess water is removed in two coalescing filters. Initially, air was dried using a dessicant dryer to achieve a water content smaller than 20 ppm. It was found, however, that the catalyst activity could not be kept constant due to fast, reversible adsorption of these traces of water. After a decrease in reactor temperature, the activity would slowly decrease. When exposing the bed to the maximum temperature of approximately 250 °C, the original activity could be brought back only partially over a period of several days. Since it is impossible to achieve the exact same conditions during catalyst pretreatment and during reactor operation in the kinetic reactors and the pilot-scale tubular reactor, it was chosen to operate at constant air humidity, at which the activity was found to be constant and reproducible. Deactivation by water is extremely fast. When deliberately adding a few drops of water to the dry reactor feed, the CO conversion and the maximum reactor temperature initially increased. This observation can only be explained if the water is absorbed almost instantaneously by the cata-

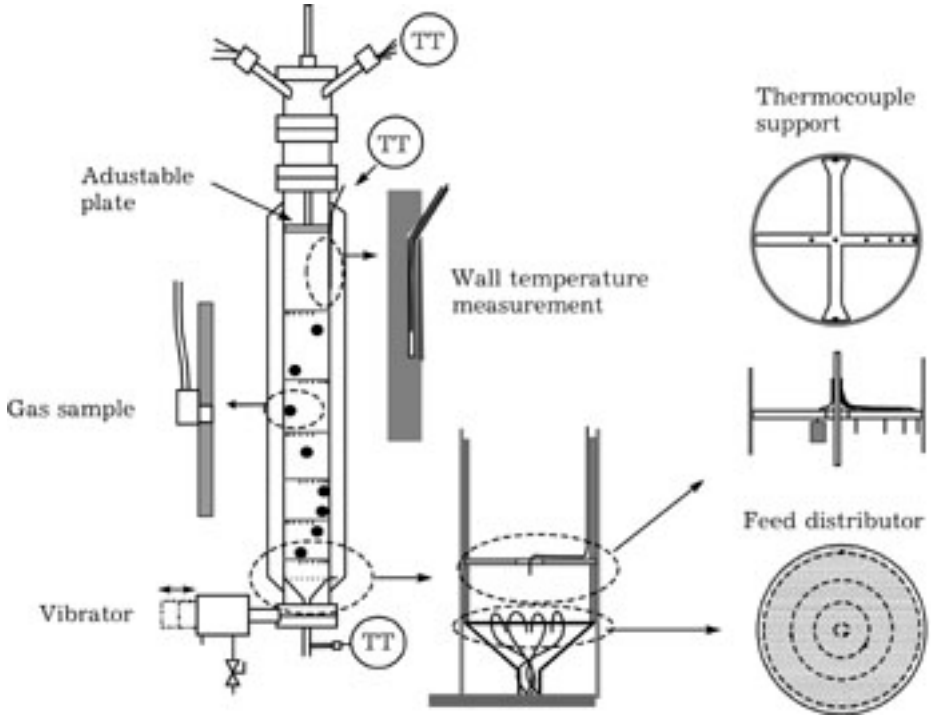

Fig. 1. Pilot scale wall-cooled tubular reactor.

lyst near the inlet. This would cause so-called 'wrong-way behavior': A decrease in the reaction rate near the entrance causes an increase of the concentration further downstream, where the temperature of the catalyst is still high. Here the reaction rate will temporarily increase, causing the overall conversion to be higher than those of the steady states before and after the perturbation.

After removal of the excess water, the air is passed through three columns filled with active carbon to remove organic contaminants. The flow of air and that of CO and CO_2 (99 % purity) was controlled by electronic mass flow controllers. Before the mass flow controller, CO was passed through a bed of SiC particles heated at 250 °C to decompose any iron carbonyls present. When operating without this filter, deposition of rust-like material was found on the catalyst particles close to the reactor inlet. After mixing, the total flow rate is measured using an impeller flow meter. Instead of relying on the mass flow controllers, the inlet concentration of CO was measured by analyzing the CO_2 concentration in a sample of the reactor effluent after passing it through a small catalyst bed in which all CO is converted. The reactor feed was preheated in a tubular oven and entered the reactor through a metal funnel. Just below the sieve plate covering this funnel, the fluid temperature was measured at 4 radial positions. The reactor wall was cooled by boiling water which pumped through the cooling jacket at 4 $m^3\ h^{-1}$ using a centrifugal pump. By varying the pressure in the cooling system, the coolant temperature could be varied between 100 and 250 °C with an accuracy of 0.3 °C. At 4 axial positions, the wall temperature was measured by thermocouples inserted into capillaries welded into slits in the reactor wall.

After pretreatment of the catalyst, which consisted of heating it at 500 °C for 30 h in dry air, the reactor was filled with 1.5 kg of it. The bed was then repacked by fluidization. The flow rate was slowly increased and decreased whilst vibrating the reactor using a pneumatically driven vibrator. During this process, catalyst particles are thoroughly mixed over the length of the reactor, as was observed in a glass reactor. A reproducible porosity of 0.42 ± 0.01 could be achieved when vibrating the reactor for one minute after abruptly stopping the air supply. The reactor setup was fully automated using a Hewlett Packard data acquisition unit coupled to a PC. This allowed series of experiments at different flow rates, wall- and inlet temperatures, concentrations and reactor pressures to be performed automatically, whilst simultaneously safeguarding the setup using the control software. After changing a setpoint, steady state was assumed to be achieved when – after a minimum period – the slope of some relevant temperatures and concentrations *versus* time had become small enough.

In case of no chemical reaction, the fluid temperature at the reactor inlet was approximately 50 °C above the wall temperature. Despite the fact that the feed distributor was insulated from the reactor wall, a non-uniform radial temperature distribution was observed at the inlet low flow rates. When calculating the effective heat transport parameters, this temperature distribution was used as boundary condition at $z = 0$. Similarly, the measured wall temperature, which showed a slight increase, was used in the boundary conditions at the reactor wall. In experiments with chemical reaction, the inlet temperature was uniform and equal to the wall temperature. After changing the reactor temperature or pressure, the reactor was flushed with air for a night to allow the water content of the catalyst to come at equilibrium with that of the fluid. When applying this procedure, experiments performed at different concentrations were very well reproducible, as is shown in Fig. 2. The CO conversion near the end of the reactor and the maximum temperature do not change when twice varying the CO inlet concentration in the same manner over a period of 40 h. Temperature and concentration profiles were found to be reproducible after repacking of the catalyst bed by fluidization, during which the catalyst is redistributed over the reactor. This means that no change of the catalytic activity over the reactor length occurred, which could be caused by fouling or exposure to different temperatures.

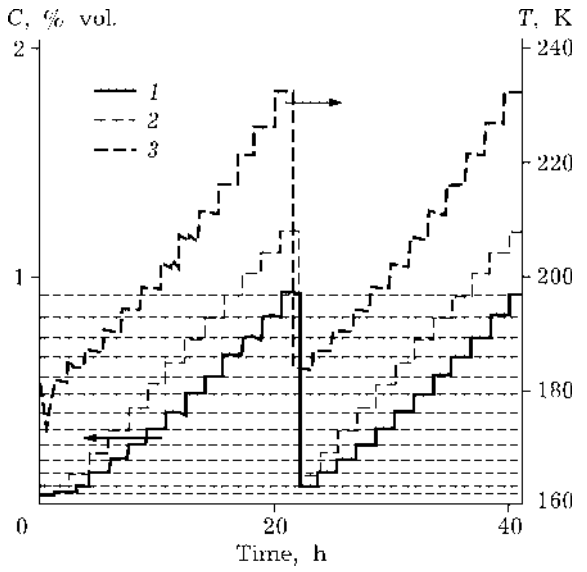

Fig. 2. Reproducibility of experiments performed at $T_{inlet} = T_{wall} = 178$ °C, $P = 3.8$ bar and a gas load of 3.55 kg m^{-2} s^{-1}: *1* – CO_2 at 610 mm, *2* – CO inlet, *3* – max *T* fluid. Shown are the maximum reactor temperature and CO_2 concentration near the bed exit as function of the CO inlet concentration. Dashed lines are drawn through CO_2 concentrations measured at the same CO inlet concentrations, which shown no inclination with respect to the horizon axis.

CATALYST PROPERTIES AND KINETICS

The used catalyst is a g-alumina extrudate containing 29 % mass copper (II) oxide. The particles have an average length of 11.5 mm and a constant diameter of 5.5 mm. An integral reactor with a length of 10 cm and an internal diameter of 8 mm, filled with a mixture of 2–5 % mass crushed catalyst (0.2 mm) and silicium carbide particles of the same size was used to study the intrinsic reaction kinetics. Experiments were performed at temperatures between 130 and 240 °C, pressures between 2 and 9 bar and fluid flow rates between 0.15 and 0.75 kg $m^{-2}s^{-1}$. The inlet concentrations of CO and CO_2 were varied between 0.1 and 1.2 and between 0.1 and 1 % vol. respectively. The overall reaction rate for the entire catalyst particles was measured in an internal recycle reactor, which is described in [12].

The reactor was modified in order to increase the maximum rotational speed of the impeller. In the original configuration, the catalyst pellets were placed inside the blades of the axial impeller used for mixing of the fluid in the reactor. During the experiments performed in this investigation, catalyst pellets with small (0.5 mm) holes were mounted on metal pins or thermocouples on ring just below the impeller. At this position, the mass and heat transfer rate between the fluid and the catalyst are smaller than in the first case.

The more important advantage is, however, that the catalyst and fluid temperatures are known accurately, making it possible to correct the measured reaction rate for particle-to-fluid heat and mass transfer limitations. In this reactor, experiments were performed at temperatures between 115 and 225 °C, pressures between 2 and 8 bar and CO and CO_2 concentrations between 0.2 and 1.4 % vol. Due to the large sensitivity of the catalyst activity to water, the same air was used as in the pilot-scale wall-cooled tubular reactor. The intrinsic kinetics of CO oxidation is described by the following Langmuir–Hinschelwood type of reaction rate expression:

$$R = \frac{k_3[\mathrm{CO}]}{1 + \frac{k_3}{k_{-6}}[\mathrm{CO}] + K_7[\mathrm{CO_2}] + K_8[\mathrm{H_2O}]} \qquad (12)$$

$$k_j = k_{0,j}\exp\left(\frac{-E_a}{RT}\right); \quad K_j = K_{0,j}\exp\left(\frac{-\Delta H_{ads}}{RT}\right)$$

Eq. (12) implies that CO reacts from the gas phase according to an Eley–Rideal mechanism. A distinction is made between CO_2 which absorbs from the gas phase on an active site (K_7 [CO_2]) and CO_2 that is present as a result of reaction of CO with adsorbed oxygen (k_3/k_{-6} [CO]). This equation has been taken from [12], with an additional term to account for the influence of the water concentration. The reaction rate measured in the integral reactor was found to decrease with increasing reactor pressure. When using intra-particle diffusion limitation to account for this decrease, the average pore size should be unrealistically small. Water adsorption does seem the only plausible explanation for the influence of pressure on the reaction rate. The overall reaction rate over the entire catalyst particles is affected by intra-particle diffusion limitation:

$$\frac{1}{V}\int_V R(C,T)\,dV = \eta R\left(C_s, T_s\right) \qquad (13)$$

C_s and T_s are the concentration and temperature at the surface of the catalyst and η is the effectiveness factor, which is a function of the size and geometry of the catalyst particles, the internal pore structure and of temperature and pressure. The effectiveness factor is approximated analytically using a method similar to that of [13], in which the particle shape is taken into account.

The effective diffusivities of CO and CO_2 were calculated from the pore size distribution measured by mercury porosimetry, combined with the results of permeation experiments using helium. The effective diffusivity is the result of weighed contributions of the different pore sizes, assuming that the pores are in parallel. Figure 3 shows a parity plot of the calculated *versus* the measured conversion for all experiments in the internal recycle reactor, together with the values of the intrinsic kinetic constants. The obtained kinetics expression accurately describes the effect of different CO_2 inlet concentrations on the temperature and concentration profiles measured in the pilot-scale wall-cooled tubular reactor.

RESULTS

Experiments without reaction have been performed using 6 catalyst beds which were obtained by catalyst repacking by fluidization. A total of 113 experiments were performed at reactor pressures between 2 and 8 bar, flow rates of 0.1 to 5.5 kg m^{-2} s^{-1}, wall temperatures between 100 and 200 °C and temperature differences of 6 to 70 °C. The effective radial thermal conductivity and wall heat transfer coefficient were optimized to minimize the difference between the measured and the calculated temperatures as:

$$f\left(\lambda_{e,r}, \alpha_w\right) = \sum_{i=1}^{n} \frac{\left(T_i^{calc} - T_i^{exp}\right)^2}{T_{r=0}^{calc} - T_{r=1}^{calc}} \qquad (14)$$

Figure 4 shows $\lambda_{e,r}/\lambda_f$ and Nu_w as function the fluid Peclet number. The dashed lines in this figure are calculated by averaging the heat transfer parameters obtained for individual experiments, whereas the solid lines were obtained by using the entire set of experimental data. In the latter case, $\lambda_{e,r}$ and α_w were assumed to comply with eqs. (8) and (11).

Both approaches agree very well, considering the non-linear differences between both averaging methods. Axial dispersion of heat, omitted in the balance equations, was found to be of negligible influence on the obtained heat transport parameters and on the target function of the minimization procedure. A possible influence of a radial velocity distribution cannot be detected when evaluating temperature fields measured without chemical, as was observed earlier by Borman *et al.* [13], who made a theoretical investigation using a two-region model. When applying a radial velocity distribution in eq. (1), assuming the fluid contribution to the effective radial thermal conductivity to be independent of the radial position, the wall heat transfer coefficient remains unchanged, whilst λ_r^f changes proportionally to the ratio of the velocity at the centerline of the reactor and the average axial

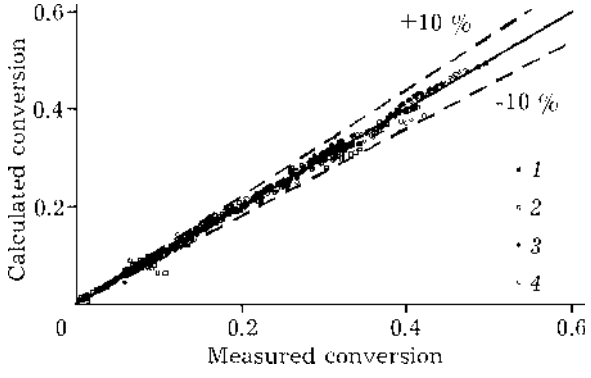

Values of parameters in eq. (12):

$k_{0,3}$	43	$kg^{-1}s^{-1}$
E_{a3}	33	kJ mol^{-1}
$k_{0,3}/k_{-0,-6}$	6.3 10^{-6}	$kg^{-1}s^{-1}$
$E_{a-6} - E_{a3}$	−49	kJ mol^{-1}
$K_{0,7}$	2.0 10^{-9}	$kg^{-1}s^{-1}$
ΔH_7	−79	kJ mol^{-1}
$K_{0,8}$	1.2 10^{-6}	$kg^{-1}s^{-1}$
ΔH_8	−60	kJ mol^{-1}
E_a apparent	50	kJ mol^{-1}
Average error	4 %	

Fig. 3. Parity plots of the reaction rate of CO oxidation over entire catalyst particles after optimization of the constants in the expression of the intrinsic reaction kinetics. *P*, bar: 2.2 (*1*), 3.6 (*2*), 5.7 (*3*), 8.2 (*4*). $K_{0,8}$ and ΔH_8 as in integral reactor.

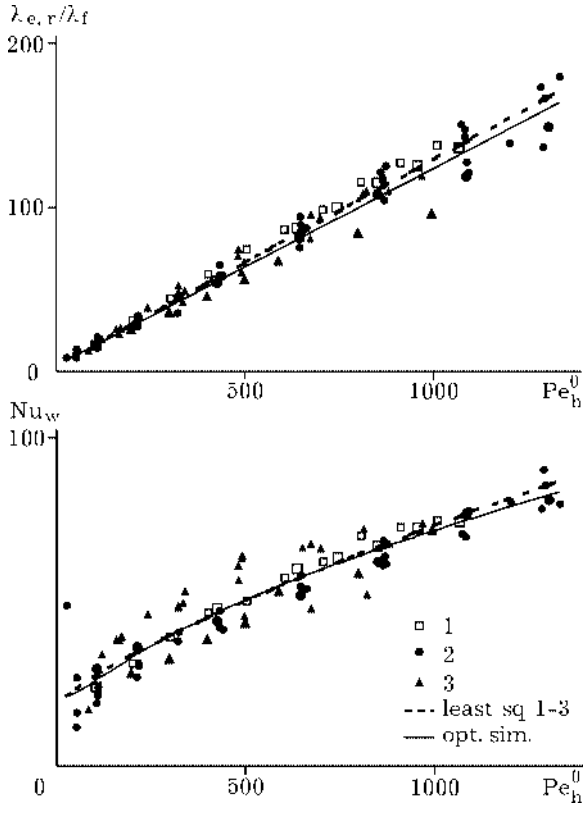

Fig. 4. Effective radial thermal conductivity and wall Nusselt number as function of the fluid Peclet number. Experiments after re-assembly of the thermocouple ladder are shown as different series.

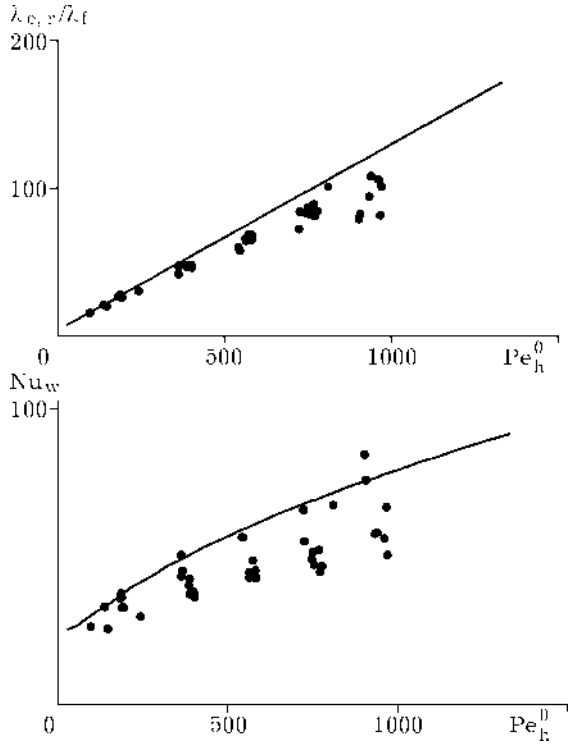

Fig. 5. Effective radial thermal conductivity and wall Nusselt number from experiments with chemical reaction at CO_{in} = 1 % vol. Lines show the heat transfer parameters obtained by optimization of eqs. (8) and (11) to all experiments without chemical reaction. $Pe_m = Pe_h$.

fluid velocity. The shape of the radial temperature profile does not depend on the shape and extent of the velocity maldistribution.

Temperature and concentration profiles with chemical reaction have been measured at Re between 200 and 1400, reactor pressures of 3, 5.9 and 8 bar and CO inlet concentrations between 0.1 and 1.5 % vol. The wall- and inlet temperatures were the same and varied between 156 and 200 °C. The maximum bed temperature was 265 °C. A fair description of the measured temperature and concentration profiles was obtained when using the independently measured reaction kinetics and the heat transfer parameters measured without reaction. In the model, radial mass transport was assumed to be analogous to radial heat transfer, so that $Pe_{m,r} = Pe_{h,r}$.

The measured temperature difference between the fluid and solid phase did agree with the predictions for the fluid-to-particle heat and mass transfer coefficient taken from [15] and [16]. However, it was found that the effective heat transfer parameters are very sensitive to the reaction kinetics. Therefore, the reaction rate was optimized to match the measured conversion. This was done by multiplying constant $k_{0,3}$ in eq. (12) by a constant. The used conversion is the maximum measured value smaller than 80 %. The maximum change of the reaction rate with respect to the reaction rate measured in the kinetic reactors is rather small and corresponds to an error in the apparent activation energy of ± 2.5 %. Figure 5 shows the effective heat transfer parameters calculated for experiments at different pressures, wall and inlet temperatures and flow rates with a CO inlet concentration of 1 % vol. At low Pe_0^f, the values of $\lambda_{e,r}$ agree with the values measured without chemical reaction. At higher fluid velocities, however, the effective radial thermal conductivity tends to become significantly smaller. After optimization of the transport parameters, the temperature profiles close to the inlet are underestimated, whilst the calculated temperatures after the hot spot are higher than measured. The discrepancy

between the heat transfer parameters with and without reaction cannot be attributed to the neglecting of heat and mass dispersion in axial direction, since their influence on the calculated profiles is negligible at the applied fluid velocities. The use of a non-uniform radial velocity distribution is the most plausible reason for the discrepancy. The effect of such velocity distribution on the predictions of the model has been investigated by [14, 17–29]. Hennecke and Schlünder [17] and Hein [27] observed a significant improvement of their model's agreement with experimental data at low Re when including a velocity distribution. The most important effect of a decreased fluid velocity at the core of the bed is the increase in the ratio of the rate heat production by reaction and the rate of heat removal through convection. The reaction rate is affected only moderately affected by radial differences in the fluid velocity. Radial concentration differences are usually much smaller than radial temperature differences and the reaction rate is much less sensitive to the concentration than it is to temperature. To improve our model, the porosity and velocity distributions will be calculated according to Giese *et al.* [30], who experimentally investigated porosity and velocity profiles for packings of spheres. For cylindrical particles with a height equal to the diameter, the following correlation for the porosity is proposed:

$$\varepsilon(r) = \varepsilon_\infty \left[1 + \left(\frac{\varepsilon_w}{\varepsilon_\infty} - 1 \right) \exp\left(-C \frac{(R_t - r)}{d_p^e} \right) \right] \quad (15)$$

in which ε_w is the porosity at the wall and ε the porosity at infinite distance from the wall, to be calculated from the known average bed porosity. For cylinders, $\varepsilon_w = 0.65$ and $C = 6$. The velocity distribution over the radius is obtained assuming radial pressure gradients to be negligible. The radial velocity distribution for different values of ε_w. $u_{r=0}/u_0$ was found not to depend on u_0 for $140 < \mathrm{Re} < 1400$.

When applying the non-uniform radial porosity and velocity distributions, the dependence of λ_r^f on r should be defined. The radial porosity distribution has two opposite effects. The increased porosity near the wall results in an increased fluid velocity and in a decreased tortuosity of the fluid path in between the catalyst pellets. These two effects oppositely influence λ_r^f at high fluid flow rates. In accordance with [3] and [17], the effects are assumed to cancel each other, so that $\lambda_{e,r}$ is constant over the radius. The reaction rate and the fluid-to-particle heat and mass transfer coefficients are corrected for the radial porosity and velocity distribution. It was found that, for constant ratio of the velocity at the core of the bed and the average fluid velocity, the model predictions are not sensitive to the exact shape of the velocity profile. Changing of the value of C in eq. (15) or even the assumption of full slip conditions at the wall does hardly affect the calculated concentration and temperature fields.

Figure 6 shows the effective heat transfer parameters with and without chemical reaction for the case $u_{r=0} = 0.85\ u_0$, corresponding to $\varepsilon_w = 0.75$. This distribution was found to give optimum agreement between the effective heat transfer parameters obtained with and without chemical reaction. $\varepsilon_w = 0.75$ is between the value suggested for the cylinders with a height-over-diameter ration of 1 and the value rec-

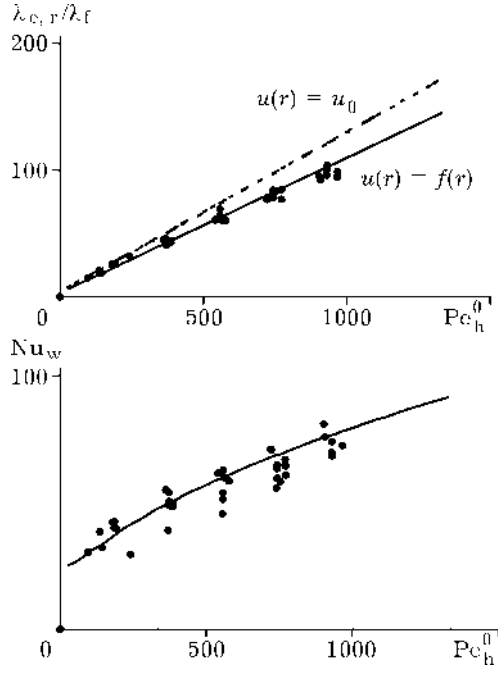

Fig. 6. As Fig. 5, with radial distribution of the axial fluid velocity. $C = 6$, $\varepsilon_w = 0.75$. $u_{r=0} = 0.85\ u_0$. Effective radial thermal conductivity in case of uniform velocity distribution is shown as dashed line.

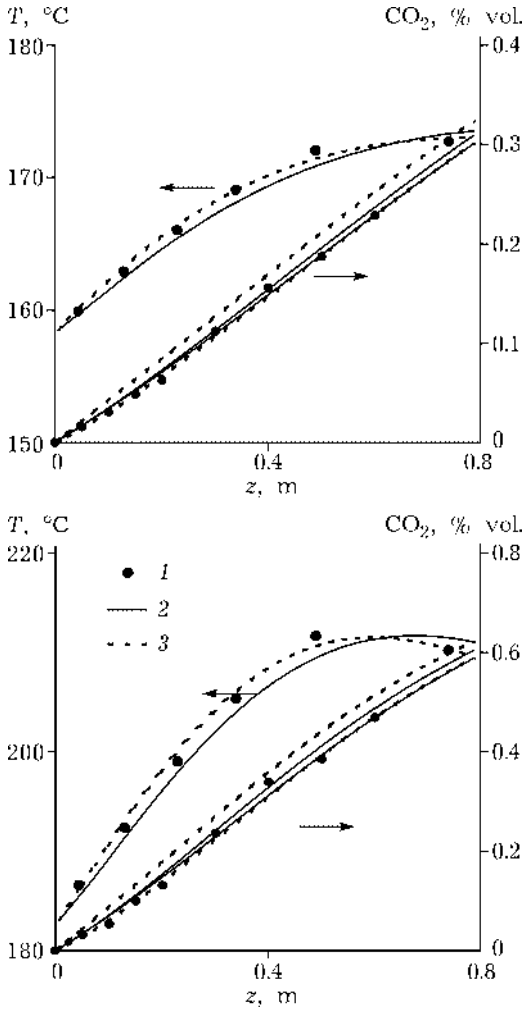

Fig. 7. Temperature at $r = 0$ and CO_2 concentration at $r = 0$ and $r = R_t$ for experiments at different wall and inlet temperatures: *1* – measured, *2* – basic model, *3* – uc/uav = 0.86. Re = 1100, P = 8 bar, CO_{in}= 1 % vol.

ommended for spheres, which is 0.87. The improvement becomes more clear when lumping $\lambda_{e,r}$ and a_w into an overall heat transfer coefficient U, which is the proportionality coefficient between the heat flux to the wall and the difference between the average bed temperature and the wall temperature.

With assumption of a radial velocity distribution, the results of the model are closer to the experimental data, as is shown in Fig. 7. The initial axial temperature gradient at the reactor inlet is not sensitive to radial heat transport, but is determined mainly by the ratio of the heat production rate and the rate of heat removal through convection. When overestimating the velocity at the core of the reactor, the initial temperature is underestimated. As a result, $\lambda_{e,r}$ is decreased during parameter estimation, causing overestimating of the temperature after the hot spot in the reactor.

CONCLUSION

Experiments performed in a pilot-scale wall-cooled tubular reactor using a wide range of operating conditions were evaluated using a two-dimensional heterogeneous reactor model. It was found that the assumption of a non-uniform radial distribution of the axial fluid velocity improves the agreement between the effective heat transport parameters obtained from experiments with and without reaction and results in a better description of the measured temperature and concentration profiles.

Notation

a – specific area per m^3 of bed, $m^2\ m^{-3}$;
a_p – surface of a particle, m^2;
C – constant or dimensionless concentration;
c – concentration component j, mol m^{-3};
c_p – heat capacity, J $kg^{-1}\ K^{-1}$;
d_p – particle diameter, m;
d_p^e, d_p – (volume-equivalent) particle diameter, m;
D – diffusion coefficient, $m^2\ s^{-1}$;
E_a – activation energy, J mol^{-1};
ΔH_{ads} – adsorption enthalpy, J mol^{-1};
ΔH_r – reaction enthalpy, J mol^{-1};
h_p – length of a cylindrical particle, m;
$K_\#$ – adsorption constant, $kg^{-1}\ s^{-1}$;
k – reaction rate constant, order n, $mol^{1-n}m^{3n}kg^{-1}s^{-1}$;
k_g – particle-to-fluid mass transfer coefficient, m s^{-1};
n – constant or reaction order;
$Pe_{h,r}$ – fluid Peclet number at fully developed turb. flow;
R – gas constant, 8.3143 J $mol^{-1}\ K^{-1}$;
R_i – reaction rate i, mol $kg^{-1}\ s^{-1}$;
R_t – bed radius, m;
r – radial coordinate, m;
r_p – radius of a cylindrical particle, m;
T – temperature, K;
t – time, s;
U – overall heat transfer coefficient, W $m^{-2}\ K^{-1}$;
u – superficial fluid velocity, m s^{-1};
v_p – volume of a particle, m^3;
z – axial coordinate, m.

Greek

α_p – particle-to-fluid heat transfer coefficient, W $m^{-2}\ K^{-1}$;

a_w – wall heat transfer coefficient, W m^{-2} K^{-1};
e – bed porosity;
e_w, e – porosity at the wall and at infinite distance from the wall;
h – dynamic viscosity, Pa s
or: effectiveness factor;
$l_{e,r}$ – effective radial thermal conductivity, W m^{-1} K^{-1};
l – thermal conductivity, W m^{-1} K^{-1};
λ_r^0 – static contribution to $l_{e,r}$, W m^{-1} K^{-1};
λ_r^f – dynamic contribution to $l_{e,r}$, W m^{-1} K^{-1};
n – stochiometry constant;
r – density, kg m^{-3}.

Dimensionless groups

Bi – Biot number for heat transfer at the wall, $a_w R_t / l_{e,r}$
Nu_w – wall Nusselt number, $\alpha_w d_p^e / \lambda_f$;
Pe_h^0 – fluid Peclet number, $u_0(\rho c_p)_f d_p^e / \lambda_f$;
$Pe_{h,r}$ – fluid Peclet number for radial heat transport, $u_0(\rho c_p)_f d_p^e / \lambda_{e,r}$;
$Pe_{m,r}$ – fluid Peclet number for mass heat transport, $u_0 d_p^e / D_{e,r}$;
Pr – fluid Prandtl number, $\eta c_{p,f} / \lambda_f$;
Re – Reynolds number, $u_0 \rho_f d_p^e / \eta$.

Sub- / superscripts

0 – average value at inlet conditions;
calc – calculated;
e – effective;
exp – experimental;
f – fluid;
h – heat;
i – reaction number;
j – component number;
m – mass;
r – radial;
s – solid.

REFERENCES

1 R. E. Hall and J. M. Smith, *Chem. Eng. Prog.*, 45 (1949) 459.
2 H. Hoffman, *Chem. Ing. Techn.*, 51 (1979) 257.
3 M. J. Schwedock, L. C. Windes, W. H. Ray, *Chem. Eng. Comm.*, 78 (1989) 45.
4 E. P. S. Schouten, P. C. Borman, K. R. Westerterp, *Chem. Eng. Sc.*, 49 (1994) 4725.
5 S. Yagi, D. Kunii, *AIChE J.*, 3 (1957) 373.
6 R. Bauer, E. U. Schlünder, *Int. Chem. Eng.*, 18 (1978) 189.
7 E. U. Schlünder, *Chem. Ing. Techn.*, 38 (1966) 967.
8 R. W. Fahien, J. M. Smith, *AIChE J.*, 1 (1955) 28.
9 V. Specchia, G. Baldi, S. Sicardi, *Chem. Eng. Comm.*, 4 (1980) 361.
10 G. Eigenberger, *Chem. Eng. Sc.*, 27 (1972) 2909.
11 A. G. Dixon, D. L. Creswell, *AIChE J.*, 25 (1979) 663.
12 P. C. Borman, A. N. R. Bos, K. R. Westerterp, *Ibid.*, 40 (1994) 862.
13 R. J. Wijngaarden, 'The scaling-up of cooled tubular reactors', Thesis, University of Twente, 1988.
14 J. G. H. Borkink, K. R. Westerterp, *Chem. Eng. Sc.*, 49 (1994) 863.
15 W. J. Beek, Drinkenburg, Proc. Int. Symp. Fluidization, Neth. Univ. Press, Amsterdam, 1967, p. 507.
16 V. Gnielinksi, Verfahrenstechnik, 16 (1982) 36.
17 F. W. Hennecke, E. U. Schlünder, *Chem. Engng. Technol.*, 45 (1973) 277.
18 O. Kalthoff, D. Vortmeyer, *Chem. Eng. Sc.*, 35 (1980) 1637.
19 D. Vortmeyer, J. Schuster, *Ibid.*, 38 (1983) 1691.
20 E. Tsotsas, E. U. Schlünder, *Ibid.*, 43 (1988) 1200.
21 D. Ziylkowski, S. Szustek, *Ibid.*, 44 (1989) 1195.
22 E. A. Foumeny H. Pahlevandahzeh, *Chem. Eng. Technol.*, 14 (1990) 161.
23 D. Vortmeyer, E. Haidegger, *Chem. Eng. Sc.*, 46 (1991) 2651.
24 I. Ziólkowska, D. Ziólkowski, *Ibid.*, 48 (1993) 3283.
25 O. Bey, G. Eigenberger, *Chem. Ing. Techn.*, 68 (1996) 1294.
26 M. A. Latifi, F. Lesage, N. Midoux, *Computers Chem. Engng.*, 22(1998) 5905.
27 S. Hein, Modellierung wandgekühlter katalytischer Festbettreaktoren mit Ein- und Zweiphasenmodellen, Fortschrittberichte VDI, Reihe 3, Nr. 593, VDI Verlag, Düsseldorf, 1999.
28 M. Winterberg, E. Tsotsas, A. Krischke, D. Vortmeyer, *Chem. Eng. Sc.*, 55 (2000) 967.
29 M. Winterberg, E. Tsotsas, *Ibid.*, 55 (2000) 5937.
30 M. Giese, K. Rottschäfer, D. Vortmeyer, *AIChE J.*, 44 (1998) 484.